The supplementary material of paper: Enhanced 3DTV Regularization and Its Applications on Hyper-spectral Image Denoising and Compressed Sensing

Jiangjun Peng, Qi Xie, Qian Zhao, Yao Wang, Yee Leung, and Deyu Meng, *Member, IEEE,*

I. The Synthetic Indian Pines HSI experiments

In order to make the comparison more fair and universal, two sets of simulation experiments were done in the text. Here are the restoration results of synthetic Indian Pines datasets. The size of the Indian pines synthetic HSI is $145 \times 145 \times 224$, which dataset has very strong local smoothness property, i.e., the structure is simple, the TV priors have proven to be more effective. Similar to DCmall datasets, we give the restoration result in these supplementary material.

Figure 1 to 2 are the visual retoration of synthetic Indian Pines dataset. In Figure 3, the distribution of evaluate index of each method are listed. Combine with the the average evaluation values of each method in the Table I, we can see that our method can achieve the best in image structure preservation and color fidelity.

To further compare the performances of all competing methods, it is necessary to show the spectral signatures before and after the restoration. In Fig. 4, the signature restoration of pixel (50, 50) in case e) are provided. In this figure, we can see that even small texture along the spectrum mode, our proposed method can also perserve.

As mentioned in the paper, for the data that have relatively simple structure and strong image smoothness property, the advantages of our method can be more obvious.

II. The Real Data Experiments

In this part, we show the restoration of other two datasets' restortation performances. From Figs. 5-8,

From the visual retoration image, it's obvious that our proposed method have achieved the best restoration performance among all competed methods.

III. Compressive Sensing

We also conduct many experiments for HSI compress sensing. In the paper, we just list two datasets' performance. Here, we list other two datasets' restoration performances.

This work was supported by GSF grants ABC123, DEF456, and GHI789. *(Corresponding author: Deyu Meng.)*

J. Yao, D. Meng, Q. Zhao and are with the School of Mathematics and Statistics and Ministry of Education Key Lab of Intelligent Networks and Network Security, Xi'an Jiaotong University, Xi'an 710049, China (e-mail: andrew.pengjj@gmail.com, {dymeng, timmy.zhaoqian}@mail.xjtu.edu.cn).

Y. Leung is the Department of Geography and Resource Management and Institute of Future Cities, The Chinese University of HongKong, Shatin, HongKong. (email: yeeleung@cuhk.edu.hk).

From 9 to 12, the different bands of different datasets are listed in the following.

Combined with the average evaluation index in tabel II, and the evaluation index distribution among bands in Figure 13. We can know that our proposed Enhanced 3DTV is universal and applicable for many types of datasets.

IV. Proof of the equivalence

We call two problems equivalent if from a solution of one, a solution of the other is readily found, and vice versa. We can then give the following theorem:

Theorem 1: For any $\mathbf{G} \in \mathbb{R}^{hw \times s}$, the problem

$$\begin{aligned} &\min_{\mathbf{V} \in \mathbb{R}^{s \times r}} \|\mathbf{G}\mathbf{V}\|_1 \\ &\text{s.t. } \|\mathbf{G}\mathbf{V}\|_F = \|\mathbf{G}\|_F, \mathbf{V}^T\mathbf{V} = \mathbf{I}, \end{aligned} \tag{1}$$

is equivalent to

$$\begin{aligned} &\min_{\mathbf{U},\mathbf{V}} \|\mathbf{U}\|_1 \\ &\text{s.t. } \mathbf{G} = \mathbf{U}\mathbf{V}^T,\ \mathbf{V}^T\mathbf{V} = \mathbf{I}, \\ &\qquad \mathbf{U} \in \mathbb{R}^{hw \times r},\ \mathbf{V} \in \mathbb{R}^{s \times r}. \end{aligned} \tag{2}$$

Proof 1:

(a). We first prove that for any $[\mathbf{U}, \mathbf{V}]$ satisfies the constrains of (2), $\mathbf{V}$ satisfies the constrains of (1).

By $\mathbf{G} = \mathbf{U}\mathbf{V}^T$ and $\mathbf{V}^T\mathbf{V} = \mathbf{I}$, we can obtain that,

$$\begin{aligned} &\|\mathbf{G}\mathbf{V}\|_F^2 = \|\mathbf{U}\mathbf{V}^T\mathbf{V}\|_F^2 = \|\mathbf{U}\|_F^2 \\ =&\text{tr}\left(\mathbf{U}^T\mathbf{U}\right) = \text{tr}\left(\mathbf{U}^{*T}\mathbf{U}\mathbf{V}^T\mathbf{V}\right) \\ =&\text{tr}\left(\mathbf{V}\mathbf{U}^T\mathbf{U}\mathbf{V}^T\right) \\ =&\|\mathbf{U}\mathbf{V}^T\|_F^2 \\ =&\|\mathbf{G}\|_F^2. \end{aligned} \tag{3}$$

This implies that $\mathbf{V}$ satisfies the constrains of (1).

(b). We then prove that for any $\mathbf{V}$ satisfies the constrains of (1), by letting $\mathbf{U} = \mathbf{G}\mathbf{V}$, $[\mathbf{U}, \mathbf{V}]$ satisfies the constrains of (2).

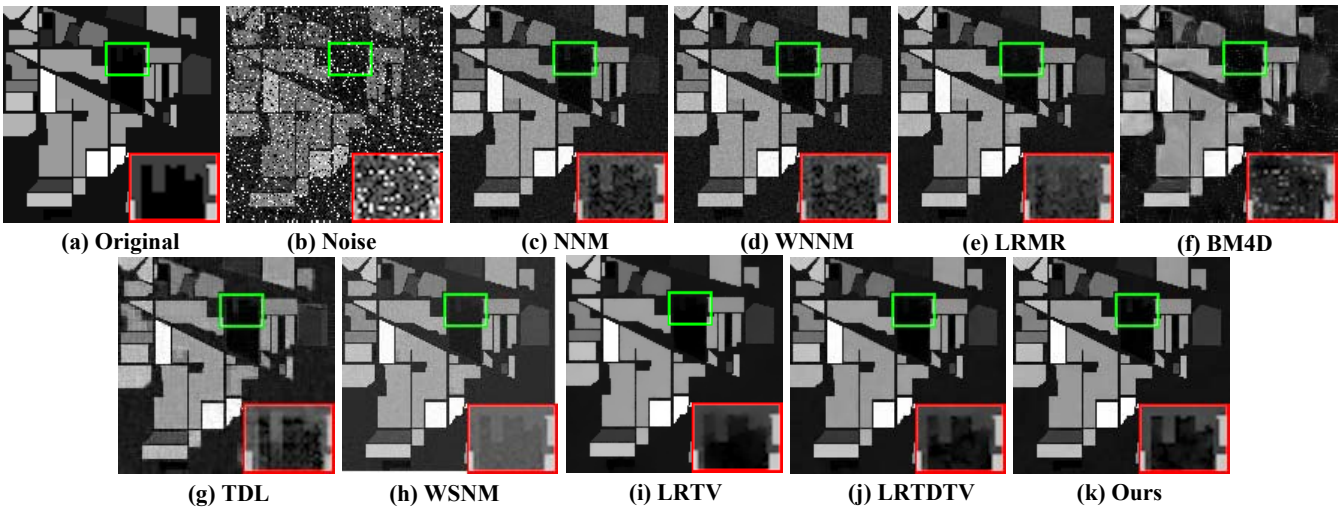

Fig. 1. Restoration performances of all competing methods on the band 220 of the ARIVIS Indian Pines HSI in case c). The demarcated area is enlarged in the right bottom corner for better visualization. The figure is better seen by zooming on a computer screen.

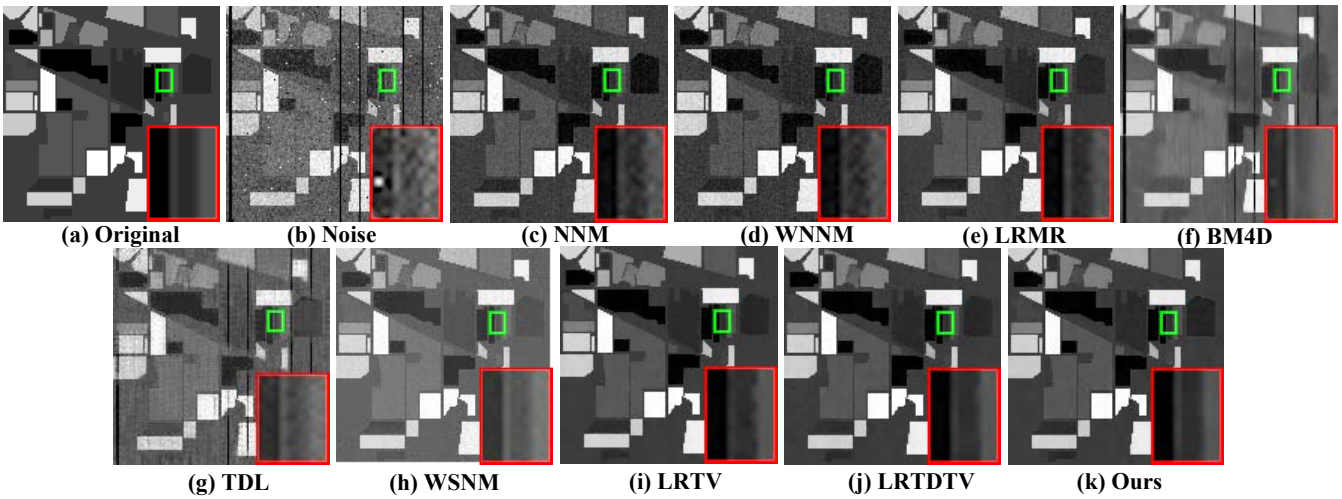

Fig. 2. Restoration performances of all competing methods on the band 120 of the ARIVIS Indian Pines HSI in case e). The demarcated area is enlarged in the right bottom corner for better visualization. The figure is better seen by zooming on a computer screen.

TABLE I
QUANTITATIVE COMPARISON OF ALL COMPETING METHODS UNDER DIFFERENT LEVELS OF NOISES IN THE INDIAN PINES DATASET. THE BEST RESULTS ARE HIGHLIGHTED IN BOLD.

Noise case	Index	Noise	NNM	WNNM	LRMR	BM4D	TDL	WSNM	LRTV	LRTDTV	Ours
Case a	PSNR	19.99	30.97	32.58	36.20	38.44	38.05	37.32	38.68	40.76	**42.33**
	SSIM	0.3672	0.8727	0.8420	0.9311	0.9763	0.9674	0.9453	0.9853	0.9804	**0.9910**
	ERGAS	233.99	69.02	57.65	36.85	29.04	30.72	32.37	28.47	**23.02**	24.32
Case b	PSNR	19.34	30.81	32.46	35.67	35.10	33.22	36.12	38.04	40.54	**41.97**
	SSIM	0.3592	0.8715	0.8415	0.9291	0.9391	0.8743	0.9402	0.9818	0.9895	**0.9910**
	ERGAS	257.88	70.06	58.39	39.84	110.40	112.35	44.89	49.18	**23.44**	24.78
Case c	PSNR	13.07	31.61	32.36	36.40	28.59	27.50	38.14	39.54	41.08	**43.13**
	SSIM	0.1778	0.8889	0.8786	0.9345	0.8401	0.9076	0.9551	0.9866	0.9910	**0.9928**
	ERGAS	520.53	64.36	59.71	36.04	90.29	102.08	29.52	35.22	**21.98**	22.55
Case d	PSNR	12.92	31.45	32.29	35.76	27.02	26.54	36.63	38.75	40.72	**42.68**
	SSIM	0.1748	0.8878	0.8777	0.9316	0.8073	0.8365	0.9485	0.9826	0.9906	**0.9926**
	ERGAS	529.82	65.45	60.10	39.99	128.11	120.54	46.32	55.44	**22.90**	23.26
Case e	PSNR	13.80	29.62	31.33	33.72	27.95	24.34	35.02	36.54	38.83	**40.80**
	SSIM	0.2038	0.8633	0.8445	0.8951	0.8201	0.5931	0.9285	0.9742	0.9859	**0.9894**
	ERGAS	500.68	81.16	66.39	50.16	121.95	158.75	51.33	72.52	28.66	**28.37**
Case f	PSNR	13.73	29.54	29.97	33.42	27.53	23.34	33.88	36.35	38.63	**40.54**
	SSIM	0.2022	0.8612	0.8431	0.8918	0.8060	0.5583	0.9261	0.9736	0.9852	**0.9888**
	ERGAS	504.37	82.18	82.48	52.62	127.28	174.28	53.29	72.05	29.82	**28.87**

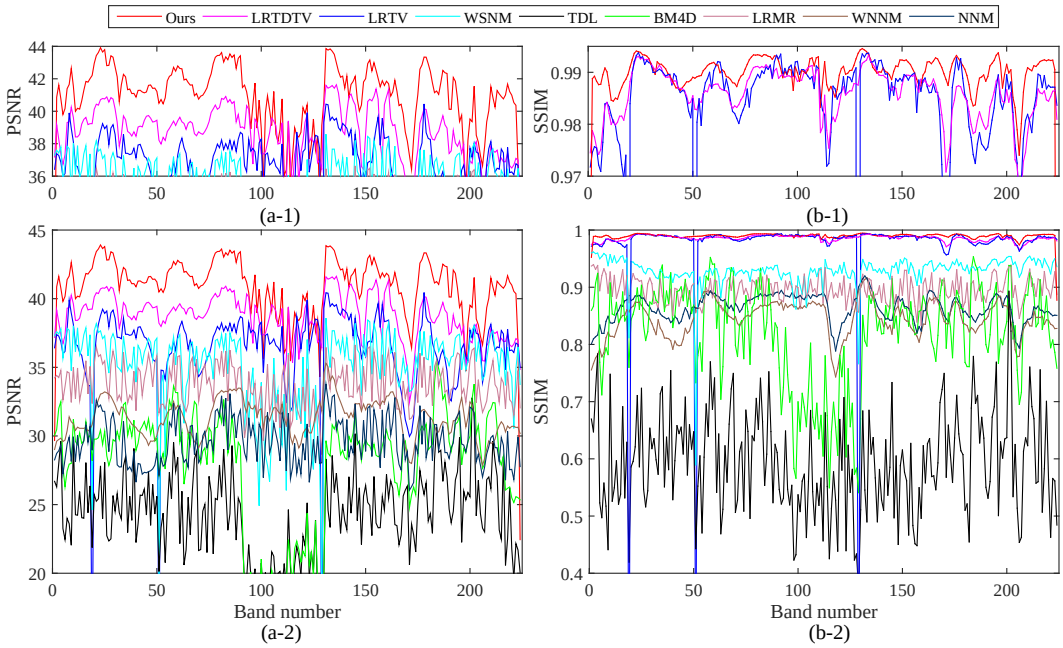

Fig. 3. Distribution of quality indices all competing methods of the ARIVIS Indian Pines HSI in case e). The curve of the bottom figure were enlarged in the top figure for better visualization on a computer screen.

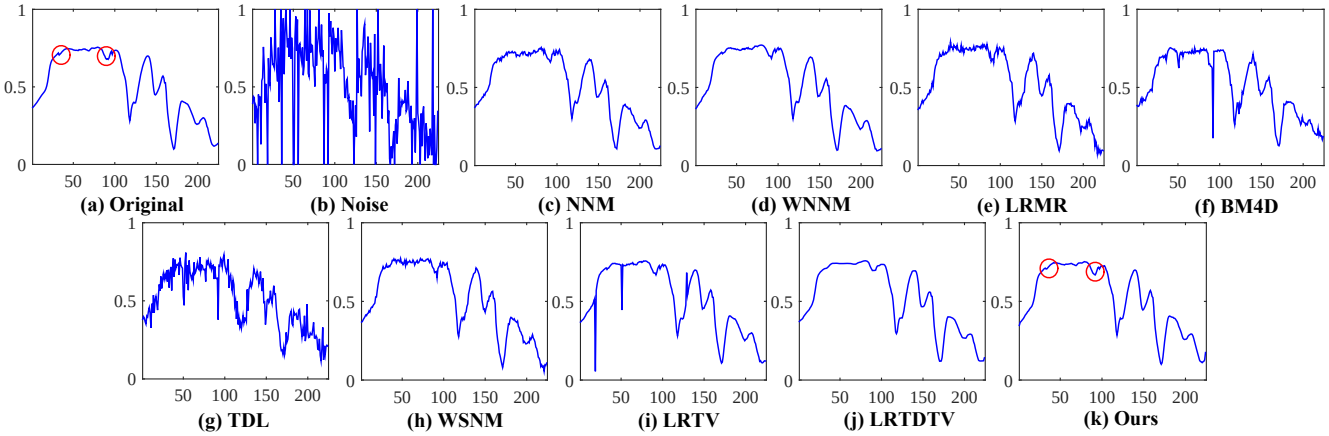

Fig. 4. Curves of spectral signatures pixel (50,50) restored by all the compared methods under ARIVIS Indian Pines HSI in case e). The detail of curve were marked by red circle to better seen on a computer screen.

By $\|\mathbf{GV}\|_F = \|\mathbf{G}\|_F$ and $\mathbf{V}^T\mathbf{V} = \mathbf{I}$, we can obtain that,

$$\begin{aligned}
&\|\mathbf{G} - \mathbf{U}\mathbf{V}^T\|_F^2 = \|\mathbf{G} - \mathbf{G}\mathbf{V}\mathbf{V}^T\|_F^2 \\
=&\mathrm{tr}\left(\mathbf{G}^T\mathbf{G}\right) - 2\mathrm{tr}\left(\mathbf{G}^T\mathbf{G}\mathbf{V}\mathbf{V}^T\right) + \mathrm{tr}\left(\mathbf{V}\mathbf{V}^T\mathbf{G}^T\mathbf{G}\mathbf{V}\mathbf{V}^T\right) \\
=&\mathrm{tr}\left(\mathbf{G}^T\mathbf{G}\right) - 2\mathrm{tr}\left(\mathbf{V}^T\mathbf{G}^T\mathbf{G}\mathbf{V}\right) + \mathrm{tr}\left(\mathbf{V}^T\mathbf{G}^T\mathbf{G}\mathbf{V}\right) \\
=&\mathrm{tr}\left(\mathbf{G}^T\mathbf{G}\right) - \mathrm{tr}\left(\mathbf{V}^T\mathbf{G}^T\mathbf{G}\mathbf{V}\right) \\
=&\|\mathbf{G}\|_F - \|\mathbf{G}\mathbf{V}\|_F \\
=&0.
\end{aligned} \tag{4}$$

Thus we have $\mathbf{G} = \mathbf{U}\mathbf{V}^T$, which implies $[\mathbf{U}, \mathbf{V}]$ satisfies the constrains of (2).

Now, it is easy to prove that for any $\mathbf{V}^*$ solves (1), then $[\mathbf{G}\mathbf{V}^*, \mathbf{V}^*]$ solves (2). If $[\mathbf{G}\mathbf{V}^*, \mathbf{V}^*]$ is not a solution of (2), then there is an $[\mathbf{U}^+, \mathbf{V}^+]$ satisfies the constrains of (2), and $\|\mathbf{G}\mathbf{V}^+\|_1 = \|\mathbf{U}^+\|_1 < \|\mathbf{G}\mathbf{V}^*\|_1$. By **(a)**, we know that $\mathbf{V}^+$ is a satisfies the constrains of (1), this is contradict to the assumption that $\mathbf{V}^*$ solves (1). Similarly, we can prove that if $[\mathbf{U}^*, \mathbf{V}^*]$ solves (2), then $\mathbf{V}^*$ solves (1). This finishes the proof.

By **Theorem 2** we know that the problem (10) and problem (11) in the maintext is equivalent to each other.

TABLE II
QUANTITATIVE COMPARISON OF ALL COMPETING METHODS UNDER DIFFERENT SAMPLING RATIO ON TWO DATASETS. THE BEST RESULTS ARE HIGHLIGHTED IN BOLD.

Data set	Sampling ratio	Quality indices	Methods					
			SpaRCS	KCS	JTTV	SLNTCS	JTenRe3DTV	ours
Moffett Field	0.3%	PSNR	26.58	23.71	27.66	24.85	29.78	**30.17**
		SSIM	0.5592	0.001	0.5975	0.0333	0.2869	**0.6995**
		ERGAS	264.89	368.24	237.38	331.08	**180.28**	182.70
	1%	PSNR	27.13	26.03	29.01	27.03	34.01	**34.19**
		SSIM	0.5691	0.0166	0.6598	0.2666	0.6198	**0.8369**
		ERGAS	256.62	295.53	206.65	257.57	**107.48**	119.19
	5%	PSNR	29.23	28.07	34.73	30.31	41.67	**43.42**
		SSIM	0.6528	0.2492	0.8559	0.4194	0.8975	**0.9713**
		ERGAS	234.04	226.74	114.02	181.53	49.37	**47.02**
	10%	PSNR	33.36	29.93	39.45	32.18	43.18	**47.72**
		SSIM	0.7374	0.4292	0.9447	0.4301	0.9223	**0.9833**
		ERGAS	210.29	217.25	65.12	178.19	42.65	**36.39**
	20%	PSNR	39.11	34.35	46.85	37.93	44.12	**49.77**
		SSIM	0.8577	0.6157	0.9861	0.8197	0.9333	**0.9868**
		ERGAS	61.08	116.60	**32.10**	68.19	38.50	33.16
Lowal Altitude	0.3%	PSNR	16.91	13.75	17.69	16.67	24.47	**24.50**
		SSIM	0.2687	0.0237	0.3412	0.0678	0.4818	**0.6357**
		ERGAS	383.13	490.69	349.63	399.84	**146.30**	148.59
	1%	PSNR	17.23	16.85	18.96	19.14	28.47	**30.76**
		SSIM	0.2821	0.1328	0.4341	0.3220	0.7344	**0.8623**
		ERGAS	374.25	387.59	304.41	272.33	98.85	**74.90**
	5%	PSNR	17.96	20.28	25.32	24.28	35.39	**38.32**
		SSIM	0.3525	0.4824	0.7534	0.6136	0.8983	**0.9526**
		ERGAS	322.52	250.12	158.30	151.82	50.03	**47.82**
	10%	PSNR	21.24	26.99	32.97	31.56	36.91	**41.24**
		SSIM	05326	0.6522	0.9151	0.8385	0.9242	**0.6490**
		ERGAS	231.86	112.80	73.35	76.41	43.64	**41.77**
	20%	PSNR	31.60	30.18	42.47	33.88	38.03	**43.05**
		SSIM	0.8517	0.7891	**0.9724**	0.8927	0.9389	0.9693
		ERGAS	104.22	81.92	**35.34**	55.43	38.34	42.82

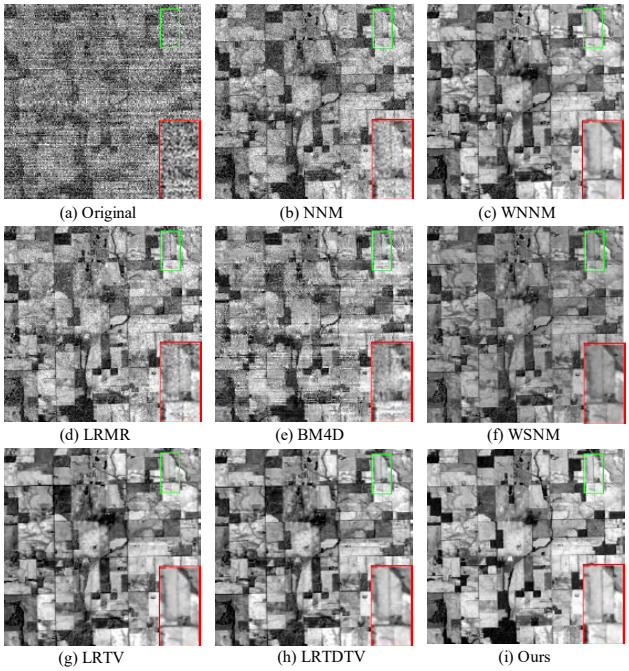

Fig. 5. Restoration performances of all competing methods on the band 109 of real Lowal HSI.

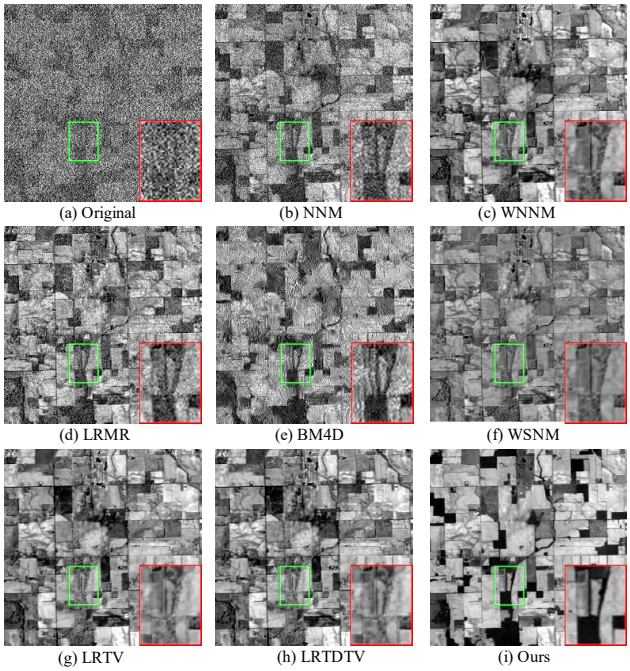

Fig. 6. Restoration performances of all competing methods on the band 162 of real Lowal HSI.

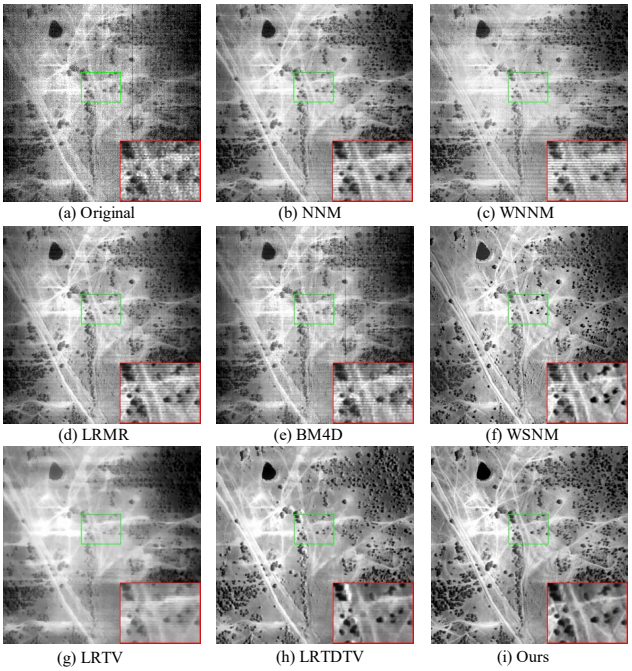

Fig. 7. Restoration performances of all competing methods on the band 104 of real Terrian HSI.

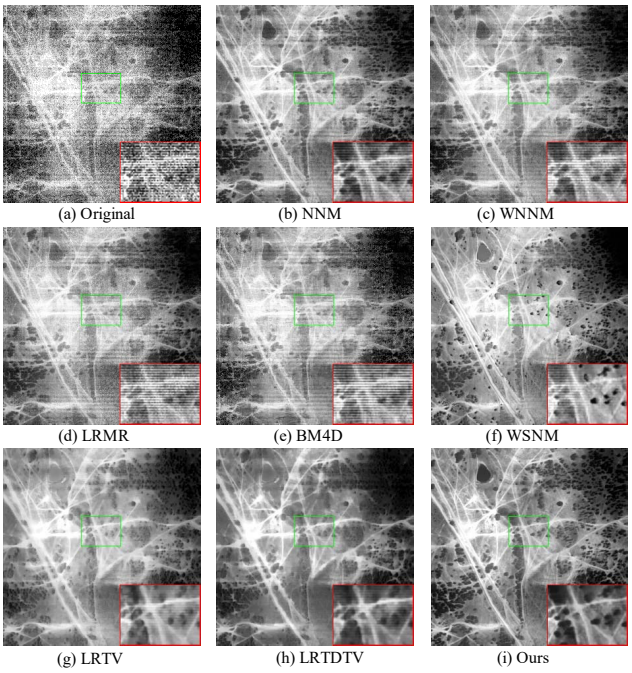

Fig. 8. Restoration performances of all competing methods on the band 151 of real Terrian HSI.

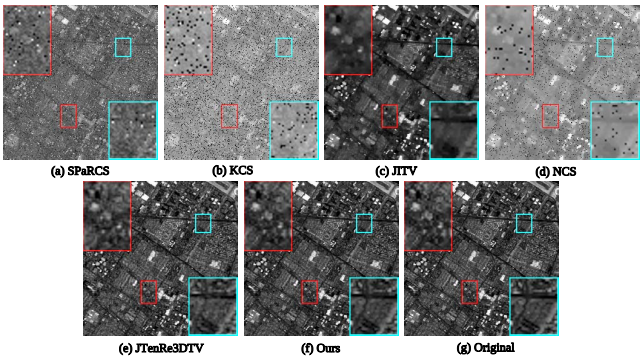

Fig. 9. Restoration performances of all competing methods on band 80 of real moffett HSI.

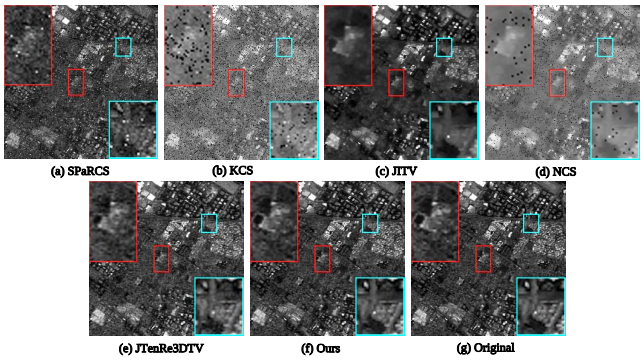

Fig. 10. Restoration performances of all competing methods on band 160 of real moffett HSI.

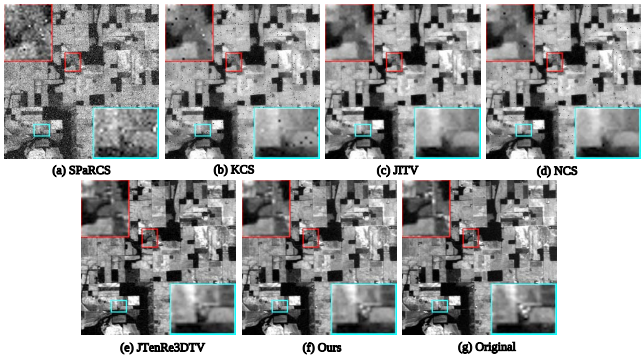

Fig. 11. Restoration performances of all competing methods on band 5 of real lowal HSI.

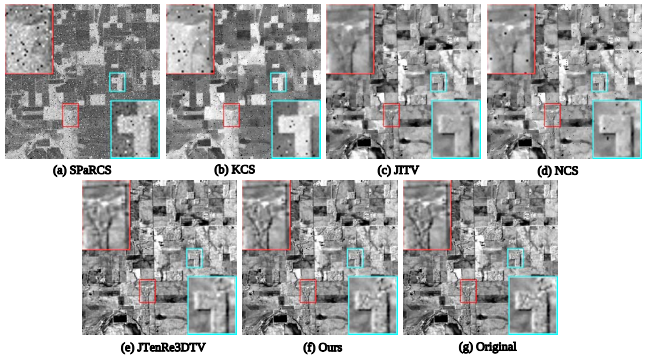

Fig. 12. Restoration performances of all competing methods on band 80 of real lowal HSI.

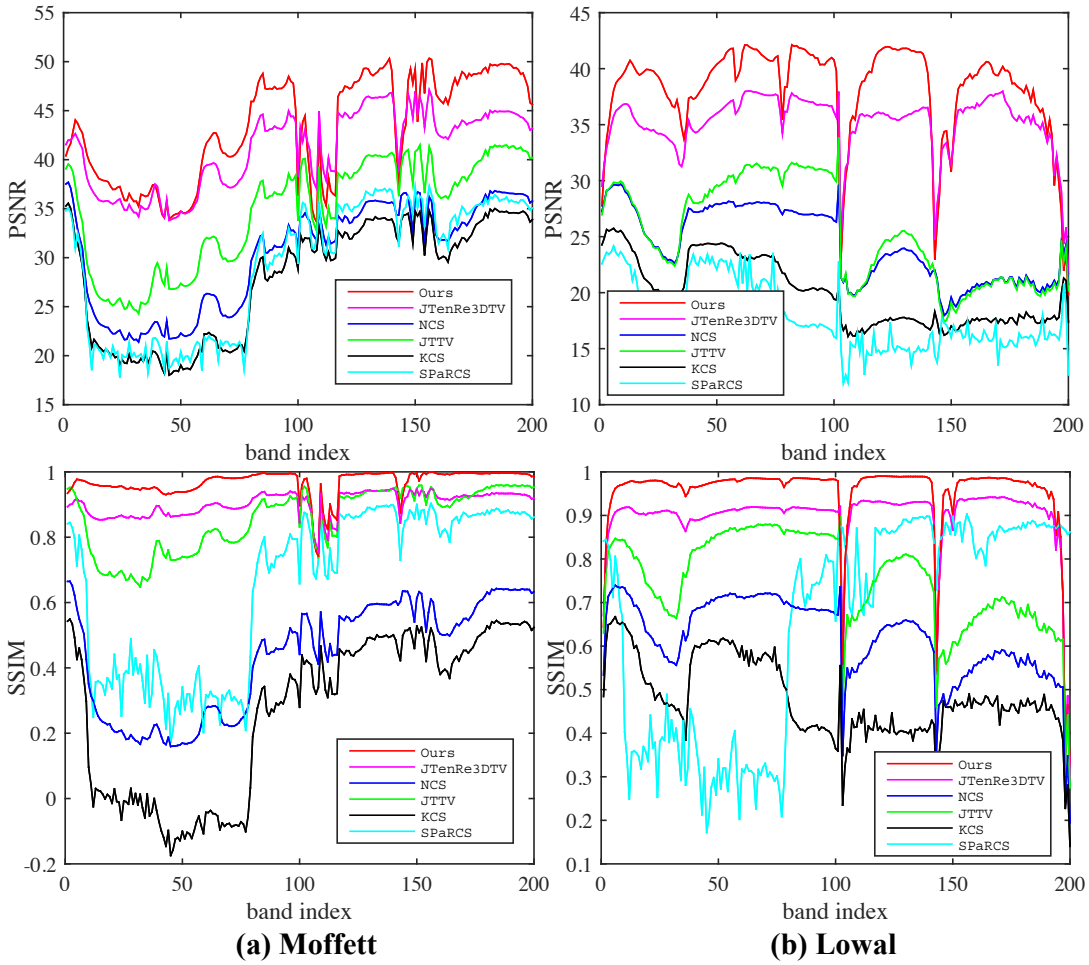

Fig. 13. The PSNR and SSIM comparisons of different methods for each band of four data sets under the sampling ratio 5%. The column from the first to the fourth correspond to the results on Moffett Field and Lowal Altitude, respectively.